

# Study of Null Geodesics and their Stability in Horndeski Black Holes

D. A. Carvajal,<sup>1,2,\*</sup> P. A. González,<sup>3,†</sup> Marco Olivares,<sup>3,‡</sup> Eleftherios Papantonopoulos,<sup>4,§</sup> and Yerko Vásquez<sup>5,¶</sup>

<sup>1</sup>*Instituto de Física, Pontificia Universidad Católica de Chile,  
Avenida Vicuña Mackenna 4860, Santiago, Chile.*

<sup>2</sup>*Departamento de Matemática y Ciencia de la Computación,  
Universidad de Santiago de Chile, Las Sophoras 173, Santiago, Chile.*

<sup>3</sup>*Facultad de Ingeniería y Ciencias, Universidad Diego Portales,  
Avenida Ejército Libertador 441, Casilla 298-V, Santiago, Chile.*

<sup>4</sup>*Physics Division, School of Applied Mathematical and Physical Sciences,  
National Technical University of Athens, 15780 Zografou Campus, Athens, Greece.*

<sup>5</sup>*Departamento de Física, Facultad de Ciencias, Universidad de La Serena,  
Avenida Cisternas 1200, La Serena, Chile.*

(Dated: March 5, 2025)

We study the motion of particles in the background of a scalar-tensor theory of gravity in which the scalar field is kinetically coupled to the Einstein tensor and we present the null geodesic structure for asymptotically flat, AdS, and dS Horndeski black holes, studying the effect of the cosmological constant on the orbits. Also, we consider three classical test of the gravity in the solar system, such as, the bending of the light, the gravitational redshift, and the Shapiro time delay in order to constraint the coupling parameters of the scalar field to gravity. Calculating the Lyapunov exponent we explore the stability of these geodesics for various values of the cosmological constant.

PACS numbers:

## Contents

<b>I. Introduction</b>	1
<b>II. Four-Dimensional Horndeski Black Hole</b>	3
<b>III. Null Geodesic structure</b>	4
A. Motion with $L = 0$	4
B. Angular motion	7
1. Bending of light	8
2. Second kind trajectories and limaçon with loop geodesic	10
3. Critical trajectories	11
4. Capture zone	11
C. Gravitational redshift	12
D. Shapiro time delay	12
<b>IV. Lyapunov exponents</b>	12
<b>V. Concluding comments</b>	13
<b>Acknowledgments</b>	14
<b>References</b>	14

## I. INTRODUCTION

Modified theories of gravity have been recently developed to address certain inconsistencies in General Relativity (GR) and to explain observations related to dark matter and dark energy. These theories propose alterations to GR at both short and large distances, aiming to offer a viable gravitational framework. Recent detections of gravitational waves (GWs) [1–5] have opened new avenues for testing alternative gravity theories and distinguishing them from GR. Therefore, it is crucial to examine the compact objects predicted by various modified gravity theories and the potential GW signatures they may produce. Additionally, investigating classical solar system tests, such as light deflection, planetary perihelion shifts, and gravitational time delays, can reveal discrepancies between GR and observational data.

Scalar-tensor theories [6], among the simplest and most extensively studied modifications of GR, introduce a scalar field coupled to gravity. This coupling leads to the formation of black holes and compact objects dressed with a hairy matter distribution. Horndeski's theory [7], a prominent scalar-tensor framework, is distinguished by second-order field equations that prevent ghost instabilities [8] and preserve classical Galilean symmetry [9, 10]. The theory has been analyzed across both short and cosmological distances. At shorter scales, subclasses featuring a scalar field kinetically coupled to the Einstein tensor admit local black hole solutions [11–15]. On cosmological scales, the derivative coupling in Horndeski theories acts as a friction term during the universe's inflationary period [16–22]. This coupling introduces a mass scale that, at large distances, can be constrained by GW observations.

\*Electronic address: [diego.carvajala@uc.cl](mailto:diego.carvajala@uc.cl)

†Electronic address: [pablo.gonzalez@udp.cl](mailto:pablo.gonzalez@udp.cl)

‡Electronic address: [marco.olivaresr@mail.udp.cl](mailto:marco.olivaresr@mail.udp.cl)

§Electronic address: [lpapa@central.ntua.gr](mailto:lpapa@central.ntua.gr)

¶Electronic address: [yvasquez@userena.cl](mailto:yvasquez@userena.cl)

In models where dark energy is represented by a scalar field coupled to the Einstein tensor, studies have shown that the propagation speed of GWs differs from the speed of light [23, 24]. This discrepancy allows for constraints on the derivative coupling parameter and serves as a test for the applicability of Horndeski theories at cosmological scales [25–31].

The measurement of the speed of GWs by GW170817 and GRB170817A provided an upper bound on the speed of GWs  $c_{gw}/c - 1 \leq 7 \times 10^{-16}$  [32]. Assuming that the peak of the GW signal and the gamma-ray burst (GRB170817A) were emitted simultaneously, a lower bound can be derived  $c_{gw}/c - 1 > -3 \times 10^{-15}$  [32], from which we can safely conclude that  $c_{gw} = c$ . Precise measurements of the propagation speed of GWs are a powerful tool for constraining the applicability of Horndeski theory. Specifically, in Horndeski theory [7] and its generalizations [33], the functions of the scalar field  $\phi$  and its kinetic energy  $X = -\frac{1}{2}\partial_\mu\phi\partial^\mu\phi$ ,  $G_4(\phi, X)$  and  $G_5(\phi, X)$  should be constrained to remain consistent with the aforementioned observations. This is because these terms provide the kinetic energy of the scalar field coupled to gravity, and they influence the speed of GWs. The term  $G_5(\phi, X)$  represents the general coupling of the scalar field to the Einstein tensor, and in [34], assuming that the scalar field plays the role of dark energy, a lower bound on the mass scale present in this term was found. Combining the constraints from inflation, the energy scale of the derivative coupling is bounded to be  $10^{15}\text{GeV} \gg M \gtrsim 2 \times 10^{-35}\text{GeV}$ .

Modified gravity theories can also be contrasted with the predictions of GR at relatively small scales. Observations within the solar system, such as light deflection, the perihelion shift of planets, and gravitational time delay, are well-explained by GR. To investigate these phenomena, one needs to compute the geodesics for particle motion around a black hole background. In [35], the perihelion precession of planetary orbits and the bending angle of null geodesics were calculated for various gravity theories in string-inspired models. The effects of gravity on the solar system have also been studied in black hole AdS geometries by analyzing the motion of particles in AdS spacetime [36–43]. The motion of both massless and massive particles in the background of four-dimensional asymptotically AdS black holes with scalar hair was explored in [44] and [45]. The geodesics were computed numerically, and the differences in the particle dynamics between the black holes with scalar hair and their no-hair limit were discussed. In the context of both solar system and astrophysical scenarios, spherically symmetric solutions arising from the coupling of the Gauss-Bonnet term with a scalar field were analyzed in [46]. Also, the motion of particles in the background of a scalar-tensor theory of gravity in which the scalar field is kinetically coupled to Einstein tensor was studied in [47], and the value of the derivative parameter was constrained through solar system tests.

Great care must be taken when studying specific

scalar-tensor theories and comparing their predictions with those of GR. In general, scalar fields, depending on their coupling to gravity, mediate fifth forces. Therefore, these theories must include a mechanism that suppresses scalar interactions at small scales, ensuring that precision tests of gravity at solar system scales remain applicable. Several screening mechanisms have been proposed to suppress scalar interactions at small scales. One of the primary screening mechanisms is the Vainshtein mechanism [48], originally developed for massive gravity (for a comprehensive review on the Vainshtein mechanism in massive gravity, see [49]). The Vainshtein mechanism also applies to Galileon-like models [9] and nonlinear massive gravity [50], where the presence of nonlinear derivative interactions in the scalar field  $\phi$  can suppress the propagation of fifth forces. In [51, 52], the consequences of the Vainshtein mechanism were studied in scalar-tensor theories, accounting for the nonlinear effects. Consequently, for modified gravity models, it is essential to understand the behavior of gravity at and below the scale at which the relevant nonlinearities arise in order to test them against experimental and cosmological observations.

A comprehensive analysis of the Vainshtein mechanism was conducted in [53], focusing on general scalar-tensor theories with second-order equations of motion in a spherically symmetric spacetime with a matter source. The study applied these general findings to specific models, including covariant and extended Galileons, as well as Dirac-Born-Infeld Galileons with Gauss-Bonnet and other terms. The results indicated that, in these theories, the fifth force can be effectively suppressed to align with solar system constraints, provided that nonlinear field kinetic terms coupled to the Einstein tensor do not dominate over other nonlinear self-interactions of the field.

The study of the motion of charged or uncharged particles outside the horizon of a black hole (BH) can give us information if these particles follow stable or unstable circular orbits. This can be done by exploring the geodesics and solving the geodesic equations. In [54, 55] the geodesics of the magnetically charged Garfinkle-Horowitz-Strominger (GHS) stringy BH [56] were studied and it was found the absence of stable circular orbits outside the event horizon for massless test particles. In the background of a magnetically charged GHS BH the motion of massive particles with electric and magnetic charges was investigated and bound and unbound orbits were found depending on critical values of the BH magnetic charge and the magnetic charge of the test particle.

All the possible trajectories around the Euler-Heisenberg (EH) BHs were studied in [57]. By studying the geodesic equations and the corresponding effective potentials it was found that the stable and unstable circular orbits of massive test particles are barely influenced by the presence of the non-linear EH electromagnetic field. However, in the case of EH AdS BH the Lyapunov exponent has been studied in [58] and it was found that chaotic bounds were found and fixing the particle charge

and changing its angular momentum these bounds were violated.

A detailed study of null geodesics was carried out in [59]. By computing the Lyapunov exponent, which is the inverse of the instability timescale associated with a geodesic motion, it was shown that in a Myers-Perry black hole background spacetime [60] in dimensions greater than four, the equatorial circular timelike geodesics are unstable, and the instability timescale of equatorial null geodesics in Myers-Perry spacetimes has a local minimum for spacetimes of dimension  $d \geq 6$ . One of the reasons of this study was that in [61] some evidence was discussed that unstable circular orbits could give information on phenomena occurring at the threshold of black hole formation in the high-energy scattering of black holes. This is obvious that this process is of great interest in fundamental physics as it was discussed in [62, 63].

The aim of this work is to study the motion of massless particles in the background of one of the most well studied scalar-tensor theory of gravity, the Horndeski theory. In this gravity theory the scalar field is kinetically coupled to the Einstein tensor and we study the null geodesic structure for asymptotically flat, AdS, and dS in the background of a Horndeski black hole. Our main purpose is to study the effect of the presence of a cosmological constant on the orbits. Also, we consider three classical test of gravity in the solar system, such as, the bending of the light, the gravitational redshift, and the Shapiro time delay in order to constraint the coupling parameters of the scalar field to gravity. Calculating also the Lyapunov exponent we explore the stability of these geodesics in the presence of a cosmological constant.

The paper is organized as follows. In Section II we give a brief review of the four-dimensional Horndeski black hole discussed in [64] which is considered as the background black hole. In Section III we study the motion of massless particles, and we establish their geodesic structure. Then, in Section IV by calculating the Lyapunov exponent we study the stability of the geodesic structure and finally, in Section V we conclude.

## II. FOUR-DIMENSIONAL HORNDESKI BLACK HOLE

In this section after reviewing the Horndeski theory we will discuss a particular hairy black hole solution [12] generated by a scalar field non-minimally coupled to the Einstein tensor. The action of the Horndeski theory [7] is given by

$$S = \int d^4x \sqrt{-g} (L_2 + L_3 + L_4 + L_5 - 2\Lambda), \quad (1)$$

where

$$L_2 = G_2(\phi, X), \quad L_3 = -G_3(\phi, X)\square\phi,$$

$$L_4 = G_4(\phi, X)\mathcal{R} + G_{4,X} [(\square\phi)^2 - (\nabla_\mu\nabla_\nu\phi)(\nabla^\mu\nabla^\nu\phi)],$$

and

$$L_5 = G_5(\phi, X)G_{\mu\nu}\nabla^\mu\nabla^\nu\phi - \frac{1}{6}G_{5,X}[(\square\phi)^3 - 3(\square\phi)(\nabla_\mu\nabla_\nu\phi)(\nabla^\mu\nabla^\nu\phi) + 2(\nabla^\mu\nabla_\alpha\phi)(\nabla^\alpha\nabla_\beta\phi)(\nabla^\beta\nabla_\mu\phi)]. \quad (2)$$

Here  $g = \det(g_{\mu\nu})$  with  $g_{\mu\nu}$  the metric tensor,  $\mathcal{R}$  and  $G_{\mu\nu}$  denotes the Ricci scalar and the Einstein tensor respectively and  $\Lambda$  is the cosmological constant. The functions  $G_i$  with  $i = 2, 3, 4, 5$  are arbitrary functions of the scalar field  $\phi$  and the kinetic term  $X = -\frac{1}{2}\partial_\mu\phi\partial^\mu\phi$ , while  $\square\phi = \nabla_\mu\nabla^\mu\phi$  is the scalar field in the d'Alembertian operator with the covariant derivative  $\nabla_\mu$ , further  $G_{j,X} = \partial G_j/\partial X$  with  $j = 4, 5$ . By considering the particular case

$$G_2 = \eta X, \quad G_4 = \zeta + \beta\sqrt{-X}, \quad \text{and} \quad G_3 = 0 = G_5, \quad (3)$$

where  $\eta$  with  $\beta$  are dimensionless positive parameters and  $\zeta = 1/2$ , the action can be written as

$$S = \int d^4x \sqrt{-g} \left( \left[ \frac{1}{2} + \beta\sqrt{(\partial\phi)^2/2} \right] \mathcal{R} - \frac{\eta}{2}(\partial\phi)^2 - \frac{\beta}{\sqrt{2}(\partial\phi)^2} [(\square\phi)^2 - (\nabla_\mu\nabla_\nu\phi)^2] - 2\Lambda \right). \quad (4)$$

A spherically symmetric BH solution [64] is given by

$$ds^2 = -f(r) dt^2 + \frac{dr^2}{f(r)} + r^2(d\theta^2 + \sin^2\theta d\phi^2), \quad (5)$$

where  $f(r)$  is the lapse function

$$f(r) = 1 - \frac{2M}{r} - \frac{\gamma^2}{r^2} - \frac{\Lambda}{3}r^2 \quad \text{with} \quad \gamma = \frac{\beta}{\sqrt{\eta}}. \quad (6)$$

From this lapse function and depending on the value of the cosmological constant  $\Lambda$ , we can study the location of the horizons by analyzing the three different configurations separately:

1. Asymptotically flat Horndeski black hole ( $\Lambda = 0$ ): The spacetime allows a unique horizon (the event horizon  $\rho_+$ ), which is located at

$$\rho_+ = M \left( 1 + \sqrt{1 + \frac{\gamma^2}{M^2}} \right), \quad (7)$$

and

$$\rho_2 = M \left( 1 - \sqrt{1 + \frac{\gamma^2}{M^2}} \right), \quad (8)$$

is a negative solution.

2. Horndeski –anti-de Sitter black hole ( $\Lambda = -\frac{3}{\ell^2} < 0$ ): The spacetime allows a unique horizon (the event horizon  $r_+$ ), which must be the real positive solution to the quartic equation

$$r^4 + \ell^2 r^2 - 2M\ell^2 r - \gamma^2 \ell^2 = 0. \quad (9)$$

Its solutions are

$$r_+ = \alpha_\ell + \sqrt{\frac{M\ell^2}{2\alpha_\ell} - \frac{\ell^2}{2} - \alpha_\ell^2}, \quad (10)$$

$$r_2 = \alpha_\ell - \sqrt{\frac{M\ell^2}{2\alpha_\ell} - \frac{\ell^2}{2} - \alpha_\ell^2}, \quad (11)$$

$$r_3 = -\alpha_\ell + \sqrt{-\frac{M\ell^2}{2\alpha_\ell} - \frac{\ell^2}{2} - \alpha_\ell^2}, \quad (12)$$

$$r_4 = -\alpha_\ell - \sqrt{-\frac{M\ell^2}{2\alpha_\ell} - \frac{\ell^2}{2} - \alpha_\ell^2}, \quad (13)$$

where

$$\alpha_\ell = \sqrt{U_\ell \cosh \left[ \frac{1}{3} \cosh^{-1} \Xi_\ell \right] - \frac{\ell^2}{6}}, \quad (14)$$

$$U_\ell = \sqrt{\frac{\ell^4}{36} - \frac{\gamma^2 \ell^2}{3}}, \quad (15)$$

$$\Xi_\ell = \frac{54M^2 \ell + 36\gamma^2 \ell + \ell^3}{(\ell^2 - 12\gamma^2)^{3/2}}. \quad (16)$$

Through the discriminant for quartic polynomials, we can find in general that this is negative for all non-zero real  $\ell$ , so these four roots are distinct; on the one hand  $r_+$  and  $r_2$  are positive and negative real roots respectively, while  $r_3$  and  $r_4$  are the complex conjugate of each other.

3. Horndeski –de Sitter black hole ( $\Lambda > 0$ ): The spacetime allows two horizons (the event horizon  $R_+$  and the cosmological horizon  $R_{++}$ ), which are obtained from the quartic equation

$$r^4 - \frac{3}{\Lambda} r^2 + \frac{6M}{\Lambda} r + \frac{3\gamma^2}{\Lambda} = 0. \quad (17)$$

Its solutions are

$$R_{++} = \alpha_\Lambda + \sqrt{-\frac{3M}{2\Lambda\alpha_\Lambda} + \frac{3}{2\Lambda} - \alpha_\Lambda^2}, \quad (18)$$

$$R_+ = \alpha_\Lambda - \sqrt{-\frac{3M}{2\Lambda\alpha_\Lambda} + \frac{3}{2\Lambda} - \alpha_\Lambda^2}, \quad (19)$$

$$R_3 = -\alpha_\Lambda + \sqrt{\frac{3M}{2\Lambda\alpha_\Lambda} + \frac{3}{2\Lambda} - \alpha_\Lambda^2}, \quad (20)$$

$$R_4 = -\alpha_\Lambda - \sqrt{\frac{3M}{2\Lambda\alpha_\Lambda} + \frac{3}{2\Lambda} - \alpha_\Lambda^2}, \quad (21)$$

where

$$\alpha_\Lambda = \sqrt{U_\Lambda \cosh \left[ \frac{1}{3} \cosh^{-1} \Xi_\Lambda \right] + \frac{1}{2\Lambda}}, \quad (22)$$

$$U_\Lambda = \sqrt{\frac{1}{4\Lambda^2} + \frac{\gamma^2}{\Lambda}}, \quad (23)$$

$$\Xi_\Lambda = \frac{18M^2\Lambda + 12\gamma^2\Lambda - 1}{(1 + 4\gamma^2\Lambda)^{3/2}}. \quad (24)$$

The roots  $R_3$  and  $R_4$  are negative solutions.

### III. NULL GEODESIC STRUCTURE

In order to study the motion of test particles in the background (5) we use the standard Lagrangian approach [36, 65, 66]. The corresponding Lagrangian is

$$2\mathcal{L} = f(r) \dot{t}^2 + \frac{\dot{r}^2}{f(r)} + r^2 \left( \dot{\theta}^2 + \sin^2 \theta \dot{\phi}^2 \right) = -m^2, \quad (25)$$

here the dot refers to derivative with respect to an affine parameter  $\lambda$ , along the trajectory, and, by normalization,  $m = 0(1)$  for massless (massive) particles. Since  $(t, \phi)$  are cyclic coordinates, their corresponding conjugate momenta  $(\Pi_t, \Pi_\phi)$  are conserved and are given by

$$\Pi_t = -f(r) \dot{t} = -E, \quad \Pi_\phi = r^2 \sin^2 \theta \dot{\phi} = L. \quad (26)$$

Therefore, by considering that the motion is performed in an invariant plane, which we fix at  $\theta = \pi/2$ , we obtain the following expressions

$$\dot{t} = \frac{E}{f(r)}, \quad \dot{\phi} = \frac{L}{r^2}. \quad (27)$$

These relations together with Eq.(25) allow us to obtain the following differential equations

$$\left( \frac{dr}{d\lambda} \right)^2 = E^2 - V_{\text{eff}}(r), \quad (28)$$

$$\left( \frac{dr}{dt} \right)^2 = [f(r)]^2 \left[ \frac{E^2 - V_{\text{eff}}(r)}{E^2} \right], \quad (29)$$

$$\left( \frac{dr}{d\phi} \right)^2 = \frac{r^4 [E^2 - V_{\text{eff}}(r)]}{L^2}, \quad (30)$$

where the effective potential  $V_{\text{eff}}(r)$ , reads

$$V_{\text{eff}}(r) = \left( 1 - \frac{2M}{r} - \frac{\gamma^2}{r^2} - \frac{\Lambda}{3} r^2 \right) \left( m^2 + \frac{L^2}{r^2} \right). \quad (31)$$

In the next sections, based on this effective potential, we analyze the null geodesic structure ( $m = 0$ ) of the spacetime characterized by the metric (5).

#### A. Motion with $L = 0$

The motion of photons with vanishing angular momentum ( $L = 0$ ) is described by a null effective potential ( $V_{\text{eff}} = 0$ ) and therefore the photons in this case can escape to spatial infinity or plunged to the horizon. Thus, the radial Eq. (28) reduces to

$$\frac{dr}{d\lambda} = \pm E, \quad (32)$$

so, an elemental integration yields

$$\lambda(r, E) = \pm \frac{r - \rho_0}{E}, \quad (33)$$

here  $\rho_0$  denotes the initial radial position of the massless particle. Note that the motion depends on the energy of the massless particle, and does not depend on the metric, thereby the above equation is valid for the three cases considered, that is, asymptotically flat, dS and AdS Horndeski spacetimes.

1. Asymptotically flat Horndeski black hole ( $\Lambda = 0$ ): by integrating Eq. (29) the coordinate time yields

$$t(r) = \pm \left[ r - \rho_0 + \frac{\rho_+^2}{\rho_+ - \rho_2} \ln \left| \frac{r - \rho_+}{\rho_0 - \rho_+} \right| - \frac{\rho_2^2}{\rho_+ - \rho_2} \ln \left| \frac{r - \rho_2}{\rho_0 - \rho_2} \right| \right]. \quad (34)$$

In Fig. 1, we show the affine parameter  $\lambda$  and the coordinate time, for a massless particle. We observe that with respect to the affine parameter the photons arrive at the horizon in a finite affine parameter, and when the photons move in the opposite direction, they require an infinity affine parameter to arrive to infinity. Also, an observer located at  $\rho_0$  will measure an infinite coordinate time for the photon to reach the event horizon. However, when the test particles move in the opposite direction,

they require a infinite coordinate time for arrive to infinity. Note that when the energy of the photon increases the affine parameter decreases.

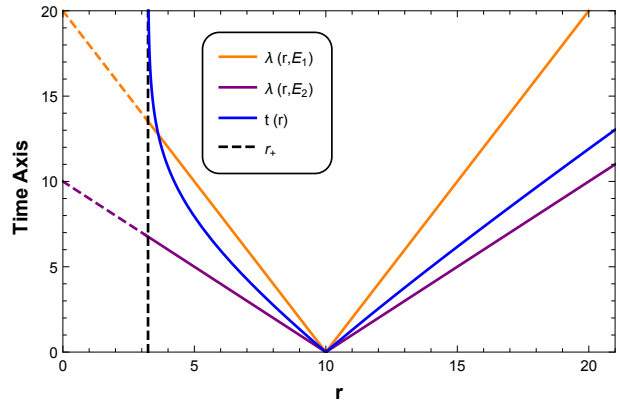


FIG. 1: Plot of the radial motion of massless particles. We have considered  $M = 1$ ,  $\Lambda = 0$ ,  $\gamma = 2$ ,  $\rho_+ = 3.236$ ,  $\rho_0 = 10$ ,  $E_1 = 0.5$ , and  $E_2 = 1$ .

2. Horndeski -de Sitter case ( $\Lambda > 0$ ): the expression for the coordinate time is

$$t_\Lambda(r) = \pm \frac{3}{\Lambda} \sum_{i=1}^4 F_i(r) \quad (35)$$

where

$$F_1(r) = \frac{-R_{++}^2}{(R_{++} - R_3)(R_{++} - R_4)(R_{++} - R_+)} \ln \left| \frac{R_{++} - r}{R_{++} - \rho_0} \right|, \quad (36)$$

$$F_2(r) = \frac{R_+^2}{(R_+ - R_3)(R_+ - R_4)(R_{++} - R_+)} \ln \left| \frac{r - R_+}{\rho_0 - R_+} \right|, \quad (37)$$

$$F_3(r) = \frac{-R_3^2}{(R_3 - R_4)(R_{++} - R_3)(R_+ - R_3)} \ln \left| \frac{r - R_3}{\rho_0 - R_3} \right|, \quad (38)$$

$$F_4(r) = \frac{R_4^2}{(R_3 - R_4)(R_{++} - R_4)(R_+ - R_4)} \ln \left| \frac{r - R_4}{\rho_0 - R_4} \right|. \quad (39)$$

3. Horndeski -Anti-de Sitter ( $\Lambda < 0$ ): in this case the coordinate time is given by

$$t_\ell(r) = \pm \ell^2 \sum_{i=1}^4 (G_i(r) - G_i(\rho_0)) \quad (40)$$

where

$$G_1(r) = \frac{r_+^2 \ln(r - r_+)}{(r_+ - r_2)(r_3 r_4 + r_+(r_+ - r_3 - r_4))}, \quad (41)$$

$$G_2(r) = -\frac{r_2^2 \ln(r - r_2)}{(r_+ - r_2)(r_3 r_4 + r_2(r_2 - r_3 - r_4))}, \quad (42)$$

$$G_3(r) = -\frac{(r_3 r_4 (r_2 + r_+) - r_2 r_+ (r_3 + r_4)) \ln(r^2 - r(r_3 + r_4) + r_3 r_4)}{2(r_3 r_4 + r_2(r_2 - r_3 - r_4))(r_3 r_4 + r_+(r_+ - r_3 - r_4))}, \quad (43)$$

$$G_4(r) = \frac{(2r_3^2 r_4^2 - r_3 r_4((r_2 + r_+)(r_3 + r_4) + 2r_2 r_+) + r_2 r_+(r_3 + r_4)^2)}{\sqrt{4r_3 r_4 - (r_3 + r_4)^2}(r_3 r_4 + r_2(r_2 - r_3 - r_4))(r_3 r_4 + r_+(r_+ - r_3 - r_4))} \times \quad (44)$$

$$\times \tan^{-1} \left( \frac{2r - r_3 - r_4}{\sqrt{4r_3 r_4 - (r_3 + r_4)^2}} \right). \quad (45)$$

In Fig. 2 we show the coordinate time, for a massless particle for the three cases considered for a fixed value of  $M$ , and  $\gamma$ . Note that for the asymptotically flat case, as we mentioned, when the test particles move to the infinity, they require a infi-

nite coordinate time to arrive to infinity. However, when the spacetime is asymptotically AdS the test particles require a finite coordinate time to arrive to infinity given by  $t_\ell(\infty) = \lim_{r \rightarrow \infty} t_\ell(r)$  which yields

$$t_\ell(\infty) = \ell^2 \left( \frac{\pi(-r_3 r_4((r_2 + r_H)(r_3 + r_4) + 2r_2 r_H) + r_2 r_H(r_3 + r_4)^2 + 2r_3^2 r_4^2)}{2(\sqrt{4r_3 r_4 - (r_3 + r_4)^2}(r_2(r_2 - r_3 - r_4) + r_3 r_4)(r_H(-r_3 - r_4 + r_H) + r_3 r_4))} \right) - (G_1(\rho_0) + G_2(\rho_0) + G_3(\rho_0) + G_4(\rho_0)). \quad (46)$$

On the other hand, when the spacetime is asymptotically dS the test particles require an infinity coordinate time in order to reach the cosmological horizon  $R_{++}$ . So, the effect of the cosmological constant is to introduce a distance limit for  $\Lambda > 0$ , and a time limit for  $\Lambda < 0$ .

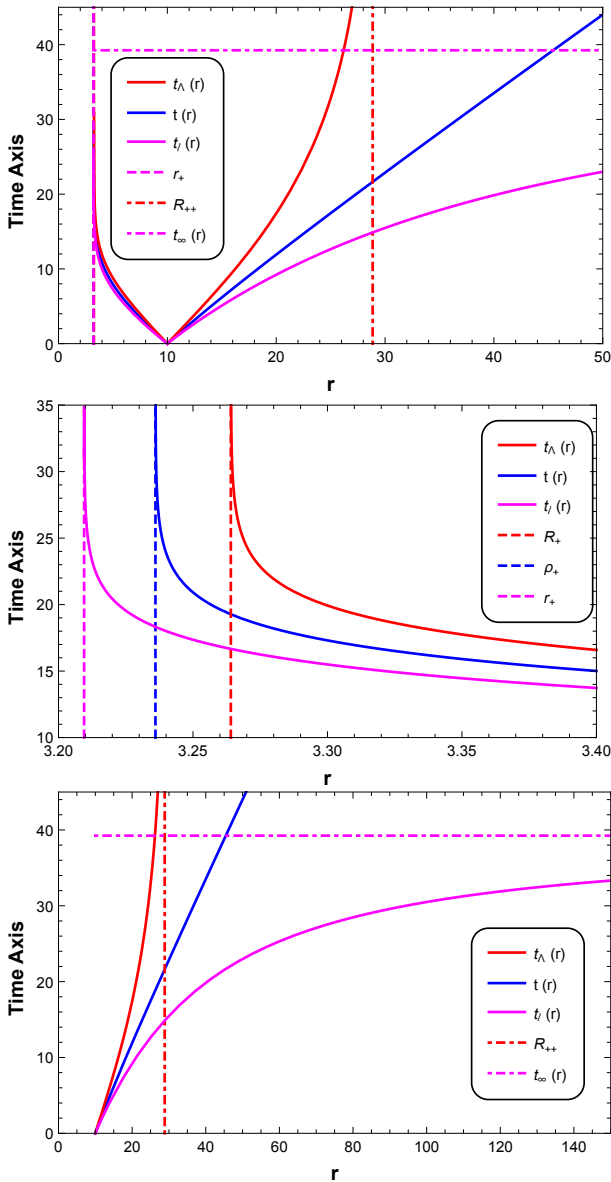


FIG. 2: Plot of the radial motion of massless particles. We have considered  $M = 1$ ,  $\Lambda = 0.003$ ,  $\ell = 30$ ,  $\gamma = 2$ ,  $\rho_0 = 10$ , so  $\rho_+ = 3.236$ ,  $r_+ = 3.209$ ,  $R_+ = 3.264$ ,  $R_{++} = 28.867$ , and  $t_\ell(\infty) = 39.246$ .

## B. Angular motion

Now, we study the motion with  $L \neq 0$ , the effective potential  $V_{\text{eff}}$  is defined by

$$V_{\text{eff}}(r) = \frac{L^2}{r^2} - \frac{2ML^2}{r^3} - \frac{\gamma^2 L^2}{r^4} - \frac{\Lambda L^2}{3}. \quad (47)$$

A typical graph of this effective potential is shown in FIG. 3, where we can observe the existence of a maximum potential located at

$$r_u = \frac{3M}{2} \left( 1 + \sqrt{1 + \frac{8\gamma^2}{9M^2}} \right), \quad (48)$$

which represents an unstable circular orbit, that is independent of the cosmological constant. Note that evaluating the effective potential Eq. (47) at  $r_u$ , given by Eq. (48), we obtain  $E_u^\ell > E_u^0 > E_u^\Lambda$ , thereby  $b_u^\ell < b_u^0 < b_u^\Lambda$ . Thus, the photon requires a greater energy for a AdS spacetime, which presents a smaller impact parameter, in order to have this kind of orbit, and a lower energy for a dS spacetime which presents a greater impact parameter. On the other hand, in Fig. 4 we plot

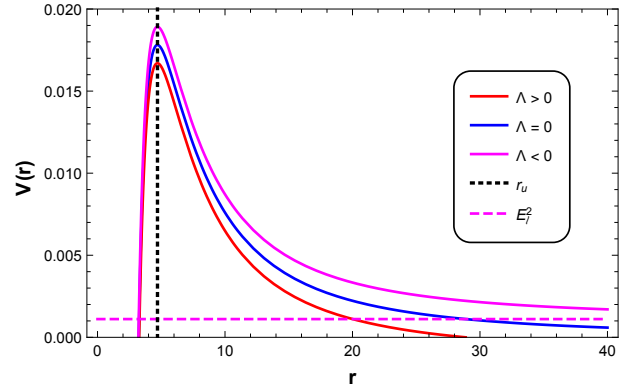


FIG. 3: Plot of the effective potential of photons. Here we have used the values  $M = 1$ ,  $\Lambda = 0.003$ ,  $\ell = 30$ ,  $\gamma = 2$ , and  $L = 1$ . The plot shows that the value of the instability distance is  $r_u = 4.702$ , where the effective potential is maximum and it is independent of the cosmological constant. Also,  $E_\ell^2 = 0.001$ .

the radial acceleration for massless particles given by  $\ddot{r} \equiv a_r(r) = -V'_{\text{eff}}(r)/2$ . We can observe the existence of a maximum radial acceleration located at

$$r_I = 2M \left( 1 + \sqrt{1 + \frac{5\gamma^2}{6M^2}} \right). \quad (49)$$

Also, note that for  $r_+ < r < r_u$ , the radial acceleration  $a_r < 0$ , for  $r = r_u$ , the radial acceleration  $a_r = 0$ , for  $r_u < r < \infty$ , the radial acceleration  $a_r > 0$ .

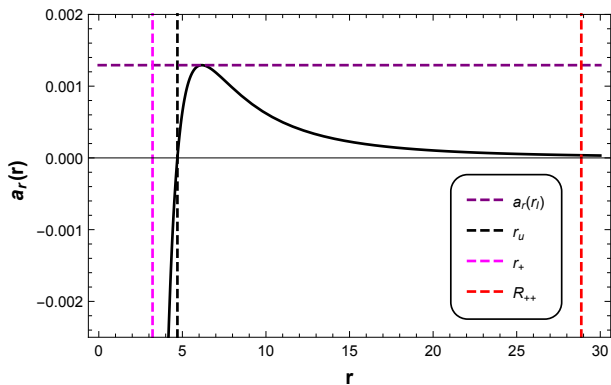


FIG. 4: Plot of the radial acceleration for massless particles. Here,  $M = 1$ ,  $\gamma = 2$ , and  $L = 1$ . The graph shows the radial acceleration, which is independent of the cosmological constant. The radial acceleration is maximum, at the inflection point,  $r_I = 6.163$ , of the effective potential. Also,  $a_r(r_I) = 0.0013$ ,  $r_u = 4.702$ ,  $r_+ = 3.209$ , and  $R_{++} = 28.867$ .

Now, in order to perform a qualitative analysis of the effective potential we will consider the impact parameter. So, by considering Eq. (30), and (47), we obtain

$$\left(\frac{dr}{d\phi}\right)^2 = \left(\frac{1}{b^2} + \frac{\Lambda}{3}\right)r^4 - r^2 + 2Mr + \gamma^2, \quad (50)$$

where  $b \equiv L/E$  is the impact parameter. Therefore, based on the impact parameter values and Fig. (3), we present a brief qualitative description of the allowed angular motions for photons in Horndeski black holes.

- (i) *Capture zone*: If  $0 < b < b_u$ , photons fall inexorably to the horizon  $r_+$ , or escape to infinity, depending on the initial conditions, and its cross section,  $\sigma$ , in this geometry is [67]

$$\sigma = \pi b_u^2 = \frac{\pi r_u^2}{f(r_u)}. \quad (51)$$

- (ii) *Critical trajectories*: If  $b = b_u$ , photons can stay in one of the unstable inner circular orbits of radius  $r_u$ . Therefore, the photons that arrive from the initial distance  $r_i$  ( $r_+ < r_i < r_u$ , or  $r_u < r_i < \infty$ ) can asymptotically fall to a circle of radius  $r_u$ . The affine period in such orbit is

$$T_\lambda = \frac{2\pi r_u^2}{L}, \quad (52)$$

and the coordinate period is

$$T_t = 2\pi b_u. \quad (53)$$

- (iii) *Deflection zone*: If  $b_u < b < b_\ell$ , this zone presents orbits of the first and second kind. The orbits of the first kind are allowed in the interval  $r_d \leq r < \infty$ , where the photons can come from a finite distance

or from an infinity distance until they reach the distance  $r = r_d$  (which is a solution of the equation  $V(r_d) = E^2$ ), and then the photons are deflected. Note that photons with  $b \geq b_\ell = \ell$  are not allowed in this zone. The orbits of the second kind are allowed in the interval  $r_+ < r \leq r_F$ , where the photons come from a distance greater than the event horizon, then they reach the distance  $r_F$  (which is a solution of the equation  $V(r_F) = E^2$ ) and then they plunge into the horizon.

- (iv) *Second kind and limaçon with loop geodesic* If  $b_u \leq b < \infty$ , the return point is in the range  $r_+ < r < r_u$ , and then the photons plunge into the horizon. However, when  $b = b_\ell$  a special geodesic can be obtained, known as the limaçon with loop.

### 1. Bending of light

Now, in order to obtain the bending of light we consider Eq. (50), which can be written as

$$\left(\frac{dr}{d\phi}\right)^2 = \frac{r^4 - \mathcal{B}^2 r^2 + 2M\mathcal{B}^2 r + \mathcal{B}^2 \gamma^2}{\mathcal{B}^2} \equiv \frac{\mathcal{P}(r)}{\mathcal{B}^2}, \quad (54)$$

where  $\mathcal{B} = \left(\frac{1}{b^2} + \frac{\Lambda}{3}\right)^{-1/2}$  is the *anomalous impact parameter*, which is a typical quantity of the anti-de Sitter spacetimes [43, 68].

Now, in order to obtain the return points, we solve the equation  $\mathcal{P}(r) = 0$ , so, the turning point is located at

$$r_d = \alpha + \sqrt{\frac{\mathcal{B}^2}{2} - \alpha^2 - \frac{M\mathcal{B}^2}{2\alpha}}, \quad (55)$$

$$r_f = \alpha - \sqrt{\frac{\mathcal{B}^2}{2} - \alpha^2 - \frac{M\mathcal{B}^2}{2\alpha}}, \quad (56)$$

$$r_3 = -\alpha + \sqrt{\frac{\mathcal{B}^2}{2} - \alpha^2 + \frac{M\mathcal{B}^2}{2\alpha}}, \quad (57)$$

$$r_4 = -\alpha - \sqrt{\frac{\mathcal{B}^2}{2} - \alpha^2 + \frac{M\mathcal{B}^2}{2\alpha}}, \quad (58)$$

where

$$\alpha = \sqrt{U_0 \cosh\left[\frac{1}{3} \cosh^{-1} \Xi_0\right] + \frac{\mathcal{B}^2}{6}}, \quad (59)$$

$$U_0 = \sqrt{\frac{\mathcal{B}^4}{36} + \frac{\gamma^2 \mathcal{B}^2}{3}}, \quad (60)$$

$$\Xi_0 = \frac{54M^2 \mathcal{B} + 36\gamma^2 \mathcal{B} - \mathcal{B}^3}{(\mathcal{B}^2 + 12\gamma^2)^{3/2}}, \quad (61)$$

$r_d$  is the deflection distance,  $r_f$  is the return point and  $r_3$  and  $r_4$  are negative solutions. Now, using Eq. (54), we obtain the quadrature

$$\phi(r) = \mathcal{B} \int_{r_d}^r \frac{dr}{\sqrt{(r-r_d)(r-r_f)(r-r_3)(r-r_4)}}. \quad (62)$$

In order to integrate out (62) it is instructive to make the change of variable  $r = r_d \left(1 + \frac{1}{4U - \alpha_d/3}\right)$ , and after

a brief manipulation, we obtain the polar trajectory of massless particles

$$r(\phi) = r_d + \frac{r_d}{4\wp(\kappa_d \phi; g_2, g_3) - \alpha_d/3}, \quad (63)$$

where  $\kappa_d = \frac{r_d}{\mathcal{B}\sqrt{u_4 u_3 u_f}}$ ,  $\alpha_d = u_4 + u_3 + u_f$ , and  $\wp \equiv \wp(y; g_2, g_3)$  is the  $\wp$ -Weierstraß function,  $g_2$  and  $g_3$  are the so-called Weierstraß invariants given by

$$\begin{aligned} g_2 &= \frac{1}{12} (u_4^2 + u_3^2 + u_f^2 - u_4 u_3 - u_4 u_f - u_f u_3), \\ g_3 &= \frac{1}{432} (2u_4 - u_3 - u_f) (2u_3 - u_4 - u_f) \cdot \\ &\quad (u_4 + u_3 - 2u_f). \end{aligned} \quad (64)$$

The other constants are:  $u_4 = \frac{r_d}{r_d - r_4}$ ,  $u_3 = \frac{r_d}{r_d - r_3}$  and  $u_f = \frac{r_d}{r_d - r_f}$ . In Fig. 5 we show the behavior of the bending of light given by Eq. (63), for a fixed value of the black hole mass  $M$ , the angular momentum  $L$ , and the parameter  $\gamma$ , we observe that the deflection angle is greater, when the black hole have a positive cosmological constant. On the other hand, note that the deflection distance,  $r_d$ , is greater, when the black hole have a negative cosmological constant.

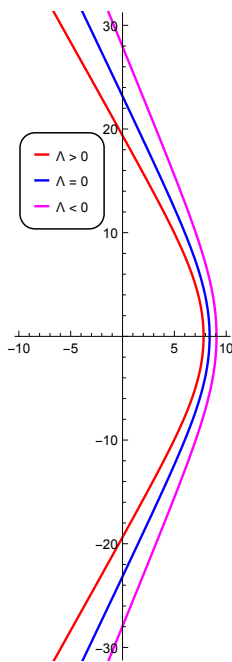


FIG. 5: Polar plot for deflection of light with  $M = 1$ ,  $\Lambda = 0.003$ ,  $\ell = 30$ ,  $\gamma = 2$ , and  $L = 1$ . All trajectories have the same energy  $E^2 = 0.01$ .

It is well known that photons can escape to infinity during a scattering process. So, by considering  $r(\phi)|_{\phi=0} = r_d$ , the shortest distance to the black hole at which the

deflection happens, and assuming that the incident photons are coming from infinity and escape to infinity, we have  $r(\phi)|_{\phi_\infty} = \infty$ . Now, by using Eq. (63) we obtain that the deflection angle,  $\hat{\alpha} = 2|\phi_\infty| - \pi$ , is given by

$$\hat{\alpha} = \frac{2}{\kappa_d} \left| \wp^{-1} \left( \frac{\alpha_d}{12}; g_2, g_3 \right) \right| - \pi. \quad (65)$$

The evolution of the deflection angle has been plotted in Fig. 6, which shows an asymptotic behavior as  $E \rightarrow E_u$ , for a fixed value of the black hole mass  $M$ , the angular momentum  $L$ , and the parameter  $\gamma$ , we can observe that the deflection angle takes an infinite value when  $E = E_u$ , such that  $E_u$  is greater, when the black hole have a negative cosmological constant. When  $E \rightarrow 0$ , the deflection angle is null for asymptotically flat, but when the cosmological constant is positive (dS) the deflection angle is a finite and not null value  $\hat{\alpha}_\Lambda(0)$ . In the case of an AdS spacetime, when  $E \rightarrow E_\ell$ , the deflection angle is null. Also, note that for a fixed value of the deflection angle, the particle requires a greater energy when the spacetime is AdS.

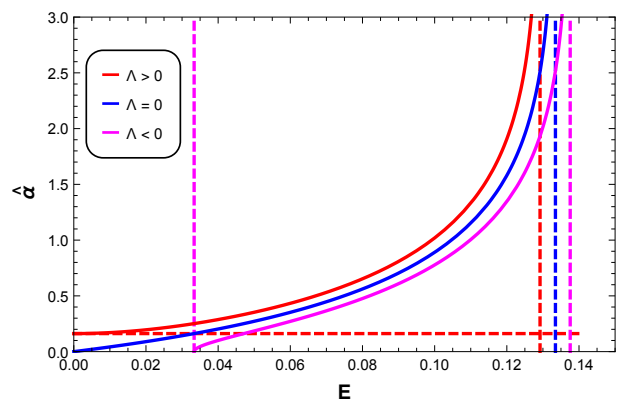


FIG. 6: The behavior of the deflection angle  $\hat{\alpha}$  in terms of  $E$ , with  $M = 1$ ,  $\Lambda = 0.003$ ,  $\ell = 30$ ,  $\gamma = 2$  and  $L = 1$ .  $E_u^0 = 0.138$ ,  $E_u^\Lambda = 0.133$ ,  $E_u^\Lambda = 0.129$ ,  $E_\ell = 0.033$ , and  $\hat{\alpha}_\Lambda(0) = 0.162$ .

The process of light deflection, or the so-called gravitational lensing, can be approached, theoretically, by means of the geodesic equations for the light rays (null geodesics). Accordingly, the first order, angular, equation of motion for the light rays (i.e. photons as the test particles) passing the black hole, is given by (50). Performing the change of variable  $r = 1/u$ , the above equation yields

$$\left( \frac{du}{d\phi} \right)^2 = \frac{1}{b^2} + \frac{\Lambda}{3} - u^2 + 2Mu^3 + \gamma^2 u^4, \quad (66)$$

that reduces to the standard Schwarzschild equation of light deflection in the limit of  $\Lambda \rightarrow 0$  and  $\gamma \rightarrow 0$ . Differentiating Eq. (66) with respect to  $\phi$ , gives

$$u'' + u = 3Mu^2 + 2\gamma^2 u^3, \quad (67)$$

where the prime denote differentiations with respect to  $\phi$ . Following the procedure established in Ref. [69], we obtain

$$u = \frac{1}{b} \sin \phi + \frac{3M}{2b^2} + \frac{\sqrt{2}\gamma^2}{2b^3} + \left( \frac{M}{2b^2} + \frac{\sqrt{2}\gamma^2}{4b^3} \right) \cos(2\phi). \quad (68)$$

Note that,  $u \rightarrow 0$  results in  $\phi \rightarrow \phi_\infty$ , with

$$-\phi_\infty = \frac{2M}{b} + \frac{3\sqrt{2}\gamma^2}{4b^2}. \quad (69)$$

The deflection angle of the light rays passing the black hole is, therefore, obtained as

$$\hat{\alpha} = 2|\phi_\infty| = \frac{4M}{b} + \frac{3\sqrt{2}\gamma^2}{2b^2}, \quad (70)$$

which recovers the famous form of  $\hat{\alpha}_{\text{Sch}} = 4M/b$  for the Schwarzschild black hole in the limit  $\gamma \rightarrow 0$ . Also, note that the constant  $\Lambda$  has no influence on the light deflection, as was pointed out in Ref. [70]. This latter, if applied for the Sun as the massive source, provides  $\hat{\alpha}_{\text{Sch}} = 4M_\odot/R_\odot = 1.75092$  arcsec. The parameterized post-Newtonian (PPN) formalism introduces the phenomenological parameter  $\tilde{\gamma}$ , which characterizes the contribution of space curvature to gravitational deflection. In this formalism the deflection angle is  $\hat{\alpha} = 0.5(1 + \tilde{\gamma})1.7426$ , and currently  $\tilde{\gamma} = 0.9998 \pm 0.0004$  [71]. So,  $\hat{\alpha} = 1.74277''$  for  $\tilde{\gamma} = 0.9998 + 0.0004$  and  $\hat{\alpha} = 1.74208''$  for  $\tilde{\gamma} = 0.9998 - 0.0004$ . The observational values, compared to the classic result, are smaller, and the contribution of the Horndeski term to the deflection angle is positive, therefore, there is not observable effect. Thus, if the Horndeski term contributes it does so that  $\hat{\alpha}_{\text{Horndeski}} < 0.00001''$ , or  $|\gamma| < 3327$  (m).

## 2. Second kind trajectories and limaçon with loop geodesic

The spacetime allows second kind trajectories, when  $b_u < b < \infty$ , where the turn point is in the range  $r_+ < r < r_u$ , and then the photons plunge into the horizon. In order to integrate out (62) from the initial distance  $r_f$  to  $r$ , it is useful to make the change of variable  $r = r_f \left(1 - \frac{1}{4U - \alpha_f/3}\right)$ , and after a brief manipulation, we obtain the polar trajectory of massless particles

$$r(\phi) = r_f - \frac{r_f}{4\wp(\kappa_f \phi; g_{2f}, g_{3f}) - \alpha_f/3}, \quad (71)$$

where  $\kappa_f = \frac{r_f}{\mathcal{B}\sqrt{u_{4f}u_{3f}u_d}}$ ,  $\alpha_f = u_d - u_{3f} - u_{4f}$  and  $\wp \equiv \wp(y; g_{2f}, g_{3f})$  is the  $\wp$ -Weierstraß function,  $g_{2f}$  and  $g_{3f}$  are the so-called Weierstraß invariants given by

$$\begin{aligned} g_{2f} &= \frac{1}{12} (u_{4f}^2 + u_{3f}^2 + u_d^2 - u_{4f}u_{3f} + u_{4f}u_d + u_d u_{3f}), \\ g_{3f} &= \frac{1}{432} (u_{3f} - u_d - 2u_{4f})(2u_{3f} - u_{4f} + u_d) \cdot \\ &\quad (u_{4f} + u_{3f} + 2u_d). \end{aligned} \quad (72)$$

The other constants are:  $u_{4f} = \frac{r_f}{r_f - r_4}$ ,  $u_{3f} = \frac{r_f}{r_f - r_3}$  and  $u_d = \frac{r_f}{r_d - r_f}$ . In Fig. 7 we show the behavior of the second kind trajectories, given by Eq. (71), for a fixed value of the black hole mass  $M$ , the angular momentum  $L$ , the energy  $E$ , and the parameter  $\gamma$ , we observe that initial distance  $r_f$  is greater when the spacetime is dS.

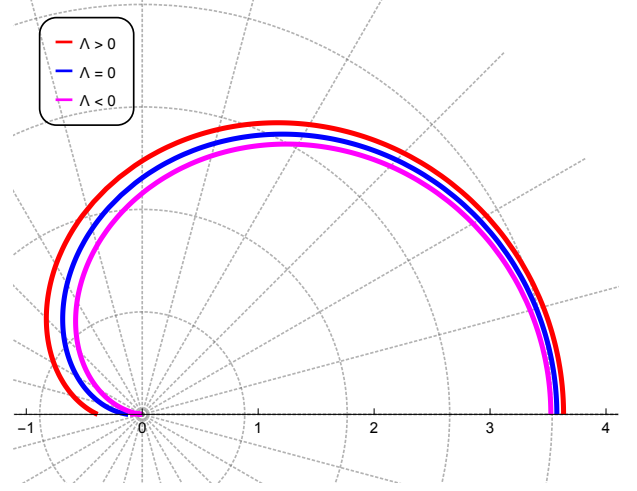


FIG. 7: Polar plot for second kind trajectories with  $M = 1$ ,  $\Lambda = 0.003$ ,  $\ell = 30$ ,  $\gamma = 2$ , and  $L = 1$ . All trajectories have the same energy  $E^2 = 0.01$ .

The AdS spacetime allows second kind trajectories, when  $b_\ell < b < \infty$ , where the turn point is in the range  $r_+ < r < r_0$ , and then the photons plunge into the horizon. However, there is a special geodesic for AdS spacetime, which can be obtained when the anomalous impact parameter  $\mathcal{B} \rightarrow \infty$  ( $b = \ell$ ). In this case, the radial coordinate is restricted to  $r_+ < r < r_0$ , and the equation of motion (50) can be written as

$$\phi = - \int_{r_0}^r \frac{dr}{\sqrt{-r^2 + 2Mr + \gamma^2}}, \quad (73)$$

and the return points are

$$r_0 = M + \sqrt{M^2 + \gamma^2}, \quad (74)$$

$$d_0 = M - \sqrt{M^2 + \gamma^2}. \quad (75)$$

Thus, it is straightforward to find the solution of Eq. (73), which is given by

$$r(\phi) = M + \sqrt{M^2 + \gamma^2} \cos \phi, \quad (76)$$

which represents the limaçon with loop geodesic of Pascal, see Fig. 8. This trajectory is a new type of orbit in Hordeski AdS, and it does not depend on the value of the cosmological constant.

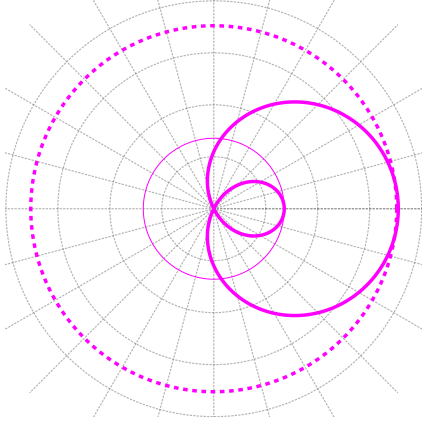


FIG. 8: The limaçon with loop geodesic (magenta line), with  $E_\ell = 0.033$ , dashed magenta lines correspond to the event horizon. Here,  $M = 1$ ,  $\ell = 30$ ,  $\gamma = 2$ ,  $L = 1$ ,  $r_0 = 3.236$ , and  $r_+ = 3.209$ .

It is worth mentioning that the analog geodesic in four-dimensional RN AdS corresponds to the limaçon of Pascal [43]. Also, when the spacetime is the five-dimensional Schwarzschild–anti-de Sitter spacetime this geodesic is given by  $r = 2M \cos \phi$ , which describes a circumference with radius  $M$  that is analog to the cardioid geodesics found in four-dimensional Schwarzschild–anti-de Sitter spacetime [36], and the Hippopede of Proclus geodesic when the spacetime is five-dimensional RNAdS [68].

### 3. Critical trajectories

In the case of  $b = b_u$ , the particles can be confined on unstable circular orbits of radius  $r_u$ . This kind of motion is indeed ramified into two cases; critical trajectories of the first kind (CFK) in which the particles come from a distant position  $r_i$  to  $r_u$  ( $r_i > r_u$ ) and those of the second kind (CSK) where the particles start from an initial point  $d_i$  at the vicinity of  $r_u$  ( $d_i < r_u$ ) and then tend to this radius by spiraling. We obtain the following equations of motion for the aforementioned trajectories:

$$r(\phi) = r_u + \frac{2(r_u - r_3)(r_u - r_4)}{(r_3 - r_4) \cosh(\kappa_u \phi + \varphi_\infty) + r_3 + r_4 - 2r_u}, \quad (77)$$

where  $\kappa_u = \frac{\sqrt{(r_u - r_3)(r_u - r_4)}}{B_u}$  and  $\varphi_\infty = \cosh^{-1}\left(\frac{2r_u - r_3 - r_4}{r_3 - r_4}\right)$ , for the first kind, and for the second kind

$$r(\phi) = r_u - \frac{2(r_u - r_3)(r_u - r_4)}{(r_3 - r_4) \cosh(\kappa_u \phi + \varphi_0) - r_3 - r_4 + 2r_u}, \quad (78)$$

where  $\varphi_0 = \cosh^{-1}\left(\frac{r_3(r_4 - r_u) + r_4(r_3 - r_u)}{r_u(r_3 - r_4)}\right)$ . In Fig. 9, we show the behavior of the CFK Eq. (77) and CSK Eq. (78) trajectories. As we mentioned,  $r_u$  is independent of the cosmological constant thereby these trajectories are the same for asymptotically flat, dS and AdS spacetime.

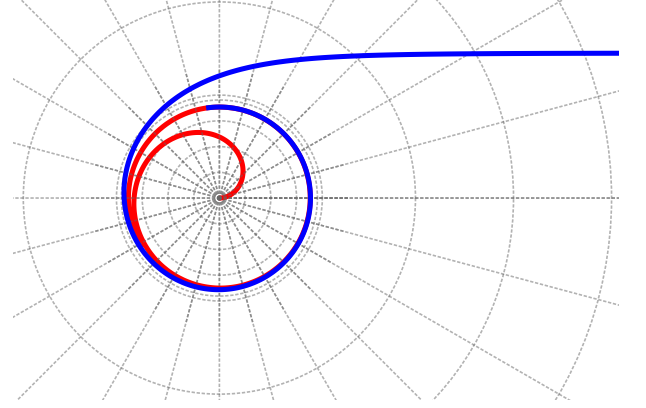


FIG. 9: The critical trajectories plotted for  $M = 1$ ,  $\gamma = 2$  and  $L = 1$ , with  $r_u = 4.7$ . Blue line for CFK and red line for CSK trajectories.

### 4. Capture zone

The photons with an impact parameter smaller than the critical one ( $b < b_u$ ), which are in the capture zone, can plunge into the horizon or escape to infinity, with a cross section given by Eq. (51). So, by manipulating Eq. (63), and by considering  $b < b_u$ , we show the trajectories of the particles in the capture zone in Fig. 10.

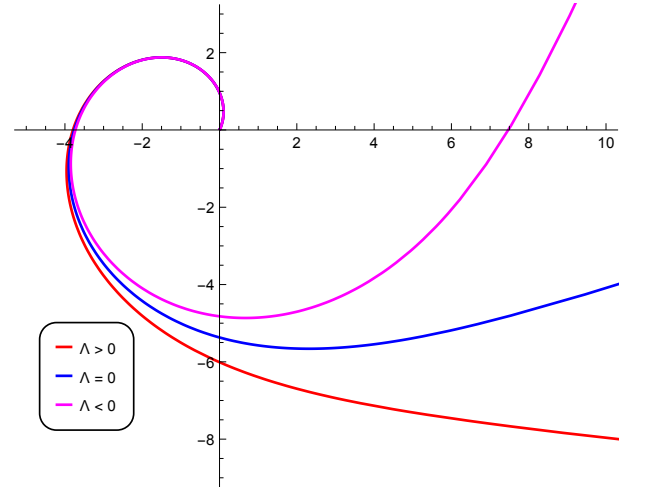


FIG. 10: The capture zone, trajectories can plunge into the horizon or escape to infinity. Here,  $M = 1$ ,  $\ell = 30$ ,  $\gamma = 2$ ,  $L = 1$ , and  $b = 7.143$ .

### C. Gravitational redshift

Since Horndeski black hole is a stationary spacetime there is a time-like Killing vector so that in coordinates adapted to the symmetry the ratio of the measured frequency of a light ray crossing different positions is given by

$$\frac{\nu}{\nu_0} = \sqrt{\frac{g_{00}(r)}{g_{00}(r_0)}}, \quad (79)$$

for  $M/(r) \ll 1$  and  $\gamma/r \ll 1$ , the above expression yields

$$\frac{\nu}{\nu_0} \approx 1 + M \left( \frac{1}{r_0} - \frac{1}{r} \right) + \frac{\gamma^2}{2} \left( \frac{1}{r_0^2} - \frac{1}{r^2} \right) + \frac{\Lambda}{6} (r_0^2 - r^2), \quad (80)$$

where we have neglected products of  $\gamma$  and  $M$ . Obviously, if we consider the limit  $M \rightarrow M_\oplus$ , and  $\gamma \rightarrow 0$ , we recover the classical result for the Schwarzschild dS and AdS spacetime. The clock can be compared with an accuracy of  $10^{-15}$ , the H-maser in the GP-A redshift experiment [72] reached an accuracy of  $10^{-14}$ . Therefore, by considering that all observations are well described within Einstein's theory with  $\Lambda = 0$ , we conclude that the extra terms of Horndeski must be  $< 10^{-14}$ . Thus,

$$|\gamma| \leq 0.945 m, \quad (81)$$

where we assume a clock comparison between Earth and a satellite at 15,000 km height, as in Ref. [70], where the authors have constrained the cosmological constant.

### D. Shapiro time delay

An interesting relativistic effect in the propagation of light rays is the apparent delay in the time of propagation for a light signal passing near the Sun, which is a relevant correction for astronomic observations, and is called the Shapiro time delay. The time delay of Radar Echoes corresponds to the determination of the time delay of radar signals which are transmitted from the Earth through a region near the Sun to another planet or spacecraft and then reflected back to the Earth. The time interval between emission and return of a pulse as measured by a clock on the Earth is

$$t_{12} = 2t(r_1, r_d) + 2t(r_2, r_d), \quad (82)$$

where  $r_d$  as closest approach to the Sun. Now, in order to calculate the time delay we use Eq. (29), and by considering that  $dr/dt$  vanishes, thereby  $\frac{E^2}{L^2} = \frac{f(r_d)}{r_d^2}$ . Thus, the coordinate time that the light requires to go from  $r_d$  to  $r$  is given by

$$t(r, r_d) = \int_{r_d}^r \frac{dr}{f(r) \sqrt{1 - \frac{r_d^2}{f(r_d)} \frac{f(r)}{r^2}}}. \quad (83)$$

So, at first order correction we obtain

$$t(r, r_d) = \sqrt{r^2 - r_d^2} + t_M(r) + t_\gamma(r) + t_\Lambda(r), \quad (84)$$

where

$$t_M(r) = M \left( \sqrt{\frac{r-r_d}{r+r_d}} + 2 \ln \left| \frac{r + \sqrt{r^2 - r_d^2}}{r_d} \right| \right), \quad (85)$$

$$t_\gamma(r) = \frac{3\gamma^2}{2r_d} \sec^{-1} \left( \frac{r}{r_d} \right), \quad (86)$$

$$t_\Lambda(r) = \frac{\Lambda}{18} (2r^2 + r_d^2) \sqrt{r^2 - r_d^2}. \quad (87)$$

Therefore, for the circuit from point 1 to point 2 and back the delay in the coordinate time is

$$\Delta t := 2 \left[ t(r_1, r_d) + t(r_2, r_d) - \sqrt{r_1^2 - r_d^2} - \sqrt{r_2^2 - r_d^2} \right], \quad (88)$$

where

$$\Delta t = 2 [t_M(r_1) + t_M(r_2) + t_\gamma(r_1) + t_\gamma(r_2)] + 2 [t_\Lambda(r_1) + t_\Lambda(r_2)]. \quad (89)$$

Now, for a round trip in the solar system, we have ( $r_d \ll r_1, r_2$ )

$$\Delta t \approx 4M \left( 1 + \ln \left| \frac{4r_1 r_2}{r_d^2} \right| \right) + \frac{3\gamma^2}{r_d} \left[ \sec^{-1} \left( \frac{r_1}{r_d} \right) + \sec^{-1} \left( \frac{r_2}{r_d} \right) \right] + \frac{2\Lambda}{9} (r_1^3 + r_2^3). \quad (90)$$

Note that if we consider the limit  $M \rightarrow M_\odot$  and  $\Lambda \rightarrow 0$ , we recover the classical result of GR; that is,  $\Delta t_{GR} = 4M_\odot \left[ 1 + \ln \left( \frac{4r_1 r_2}{r_d^2} \right) \right]$ . For a round trip from the Earth to Mars and back, we get (for  $r_d \ll r_1, r_2$ ), where  $r_1 \approx r_2 = 2.25 \times 10^{11}$  m. is the average distance Earth-Mars. Considering  $r_d$ , as closest approach to the Sun, like the radius of the Sun ( $R_\odot \approx 6.960 \times 10^8$  m) plus the solar corona ( $\sim 10^9$  m),  $r_d \approx 1.696 \times 10^9$  m, then, the time delay is  $\Delta t_{GR} \approx 240 \mu s$ . To give an idea of the experimental possibilities, we mention that the error in the time measurement of a circuit during the Viking mission was only about  $10 ns$  [69]. If the Horndeski term contributes,  $\Delta t_{Horndeski} = \frac{3\gamma^2}{r_d} \left[ \sec^{-1} \left( \frac{r_1}{r_d} \right) + \sec^{-1} \left( \frac{r_2}{r_d} \right) \right]$ , it does so that  $\Delta t_{Horndeski} < 10^{-8} s$ , or  $|\gamma| < 1.345$  (m).

## IV. LYAPUNOV EXPONENTS

Lyapunov exponents are a measure of the average rate at which nearby trajectories converge or diverge in the phase space. Thus, in order to calculate the Lyapunov exponent, we use the Jacobian matrix method [59, 73, 74].

So, taking the phase space  $(r, \pi_r)$  the Jacobian matrix  $K_{ij}$  is

$$K_{11} = \frac{\partial F_1}{\partial r}, K_{12} = \frac{\partial F_1}{\partial \pi_r}, K_{21} = \frac{\partial F_2}{\partial r}, K_{22} = \frac{\partial F_2}{\partial \pi_r}, \quad (91)$$

where  $F_1(r, \pi_r) = \frac{dr}{dt}$ , and  $F_2(r, \pi_r) = \frac{d\pi_r}{dt}$ . When the circular motion of particles is considered  $\pi_r = 0$ , and the Jacobian matrix which can be reduce to

$$K_{ij} = \begin{pmatrix} 0 & K_{12} \\ K_{21} & 0 \end{pmatrix} \quad (92)$$

being the eigenvalues of the Jacobian matrix the Lyapunov exponent  $\lambda$

$$\lambda = \sqrt{K_{12}K_{21}}. \quad (93)$$

If  $\lambda^2 > 0$  the circular motion is unstable, if  $\lambda^2 = 0$  the circular motion is marginal, and if  $\lambda^2 < 0$  the circular motion is stable. So, for circular null geodesics the Lyapunov exponent is given by [59]

$$\lambda = \frac{1}{\sqrt{2}} \sqrt{-\frac{r_u^2 f_u}{L^2} V''_{\text{eff}}(r_u)}. \quad (94)$$

In Fig. 11 we plot the Lyapunov exponent as a function of  $\ell$ . Note that for the spacetimes considered, the exponent is positive, for a fixed value of  $M$ , and  $\gamma$ , which indicates a divergence between nearby trajectories, i.e., a high sensitivity to initial conditions. So, once circular orbit is perturbed, the perturbation will increase exponentially, which indicates the presence of chaos. In the figure, the dashed red line indicates that the solution does not represent a black hole solution for the values of  $0 < \ell < 7.494$ .

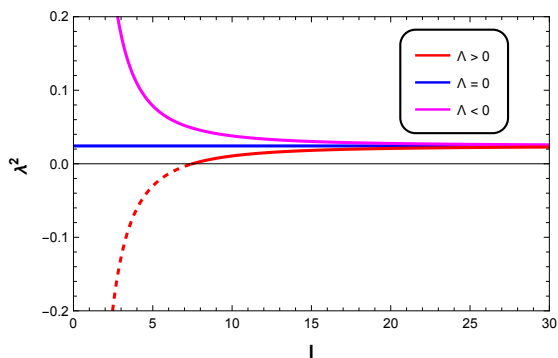


FIG. 11: The Lyapunov exponent  $\lambda^2$  as a function of  $\ell$ . Here,  $M = 1$ , and  $\gamma = 2$ .

It is worth to mentioning that a general upper bound of chaos in quantum systems has been proposed by Maldacena, Shenker and Stanford from the quantum field

theory, which indicates that the Lyapunov exponent  $\lambda$ , describing the strength of chaos, has a temperature-dependent upper bound [75]

$$\lambda \leq \frac{2\pi T}{\hbar} \quad (95)$$

This temperature-dependent ansatz was examined by shock wave gedanken-experiments [76, 77] and the AdS/CFT correspondence [78]. With the black hole thermodynamic relationship  $\kappa = 2\pi T$  and setting  $\hbar = 1$ , the chaos bound Eq.(95) has an equivalent form at the horizon

$$\lambda \leq \kappa \quad (96)$$

where  $\kappa$  is the surface gravity of black holes.

## V. CONCLUDING COMMENTS

We considered four-dimensional asymptotically flat, dS and AdS Horndeski black holes and we analyzed the motion of massless particles in these background with the objective to study the geodesics and we discuss about the effect of the cosmological constant on the motion of particles.

For the spacetimes considered we have obtained the horizons analytically. The asymptotically flat spacetime is characterized by two roots, one of them corresponds to the event horizon and the other one is negative, the dS spacetime is characterized by four roots, the event horizon, the cosmological horizon and two negative roots, and the AdS spacetime is characterized by four roots, one of them corresponds to the event horizon, the other one is negative, and two complex conjugate roots.

Concerning to the motion with  $L = 0$ , we have found that the affine parameter  $\lambda$  depends on the energy of the massless particle, and does not depend on the metric. While that for coordinate time, always the test particles require a infinite coordinate time to arrive to the event horizon. However, for  $\Lambda = 0$ , the test particles require a infinite coordinate time to arrive to infinity. On the other hand, when the spacetime is dS the test particles require a infinity coordinate time in order to reach the cosmological horizon  $R_{++}$ , and when the spacetime is AdS the test particles require a finite coordinate time to arrive to infinity. So, the effect of the cosmological constant is to introduce a distance limit for  $\Lambda > 0$ , and a time limit for  $\Lambda < 0$ .

Concerning to the angular null geodesics, firstly we have performed a qualitative analysis of the effective potential in order to identify the different kind of orbits allowed, and we have shown that the radial acceleration does not depend on the cosmological constant with a maximum in the inflection point of the effective potential. One of the allowed orbits is the unstable circular

orbit, which depend on  $M$ , and  $\gamma$ , and does not depend on the cosmological constant. However, the energy of the particle to reach this orbit meets  $E_u^\ell > E_u^0 > E_u^\Lambda$ . Here, the analysis of the Lyapunov exponent shows that the exponent is positive for the spacetimes considered, which indicates a divergence between nearby trajectories, and the presence of chaos. Other kind of trajectories are of first kind where we study the bending of the light, and we have found exact solutions for the trajectories, the return points, and the deflection distance. Also, we have found the deflection angle  $\hat{\alpha}$ , where for the spacetimes considered  $\hat{\alpha} \rightarrow \infty$ , when  $r_d \rightarrow r_u$ . Also,  $\hat{\alpha} \rightarrow 0$ , when  $E \rightarrow 0$  ( $\Lambda = 0$ ),  $\hat{\alpha} \rightarrow \hat{\alpha}_\Lambda(0)$ , when  $E \rightarrow 0$  ( $\Lambda > 0$ ), and  $\hat{\alpha} \rightarrow 0$ , when  $E \rightarrow E_\ell$  ( $\Lambda < 0$ ). The deflection angle is greater, when the black hole has a positive cosmological constant.

Also, we have completed the geodesics structure for massless particle by considering the relativistic orbits,

such as, the second kind trajectories, the critical trajectories and the geodesics of the capture zone. Mainly, we have found a new kind of second kind trajectories given by the limaçon with loop, for AdS spacetimes.

Additionally, we have considered three classical test of gravity in the solar system in order to constraint the  $\gamma$  parameter. Thus, for the bending of the light  $|\gamma| < 3327$  (m), for the gravitational redshift  $|\gamma| \leq 0.945$  (m), and for the Shapiro time delay  $|\gamma| < 1.345$  (m).

### Acknowledgments

This work is partially supported by ANID Chile through FONDECYT Grant N<sup>o</sup> 1220871 (P.A.G., and Y. V.).

- 
- [1] LIGO Scientific and Virgo Collaborations collaboration, B. P. Abbott et al., Observation of Gravitational Waves from a Binary Black Hole Merger, *Phys. Rev. Lett.* **116** (2016) 061102.
- [2] VGW151226: Observation of Gravitational Waves from a 22-Solar-Mass Binary Black Hole Coalescence, *Phys. Rev. Lett.* **116** (2016) 241103.
- [3] VIRGO, LIGO SCIENTIFIC collaboration, B. P. Abbott et al., GW170104: Observation of a 50-Solar-Mass Binary Black Hole Coalescence at Redshift 0.2, *Phys. Rev. Lett.* **118** (2017) 221101.
- [4] Virgo, LIGO Scientific collaboration, B. P. Abbott et al., GW170814: A Three-Detector Observation of Gravitational Waves from a Binary Black Hole Coalescence, *Phys. Rev. Lett.* **119** (2017) 141101.
- [5] Virgo, LIGO Scientific collaboration, B. P. Abbott et al., GW170817: Observation of Gravitational Waves from a Binary Neutron Star Inspiral, *Phys. Rev. Lett.* **119** (2017) 161101.
- [6] Y. Fujii, K. Maeda, *The scalar-tensor theory of gravitation* (Cambridge University Press, 2007).
- [7] G.W. Horndeski, Second-order scalar-tensor field equations in a four-dimensional space. *Int. J. Theor. Phys.* **10**, 363 (1974).
- [8] M. Ostrogradsky, Mémoires sur les équations différentielles, relatives au problème des isopérimètres. *Mem. Acad. St. Petersburg* **6**(4), 385 (1850).
- [9] A. Nicolis, R. Rattazzi, E. Trincherini, The Galileon as a local modification of gravity. *Phys. Rev. D* **79**, 064036 (2009).
- [10] C. Deffayet, G. Esposito-Farese, A. Vikman, Covariant Galileon. *Phys. Rev. D* **79**, 084003 (2009).
- [11] T. Kolyvaris, G. Koutsoumbas, E. Papantonopoulos, G. Siopsis, Scalar Hair from a Derivative Coupling of a Scalar Field to the Einstein Tensor. *Class. Quant. Grav.* **29**, 205011 (2012)
- [12] M. Rinaldi, “Black holes with non-minimal derivative coupling,” *Phys. Rev. D* **86**, 084048 (2012) [arXiv:1208.0103 [gr-qc]].
- [13] T. Kolyvaris, G. Koutsoumbas, E. Papantonopoulos, G. Siopsis, Phase Transition to a Hairy Black Hole in Asymptotically Flat Spacetime. *JHEP* **11**, 133 (2013)
- [14] E. Babichev, C. Charmousis, Dressing a black hole with a time-dependent Galileon. *JHEP* **08**, 106 (2014)
- [15] C. Charmousis, T. Kolyvaris, E. Papantonopoulos, M. Tsoukalas, Black Holes in Bi-scalar Extensions of Horndeski Theories. *JHEP* **07**, 085 (2014)
- [16] L. Amendola, “Cosmology with nonminimal derivative couplings,” *Phys. Lett. B* **301**, 175 (1993) [arXiv:gr-qc/9302010].
- [17] S. V. Sushkov, “Exact cosmological solutions with non-minimal derivative coupling,” *Phys. Rev. D* **80**, 103505 (2009) [arXiv:0910.0980 [gr-qc]].
- [18] C. Germani, A. Kehagias, UV-Protected Inflation. *Phys. Rev. Lett.* **106**, 161302 (2011)
- [19] E.N. Saridakis, S.V. Sushkov, Quintessence and phantom cosmology with non-minimal derivative coupling. *Phys. Rev. D* **81**, 083510 (2010)
- [20] Y. Huang, Q. Gao, Y. Gong, The Phase-space analysis of scalar fields with non-minimally derivative coupling. *Eur. J. Phys. C* **75**, 143 (2015)
- [21] N. Yang, Q. Fei, Q. Gao, Y. Gong, Inflationary models with non-minimally derivative coupling. *Class. Quant. Grav.* **33**(20), 205001 (2016)
- [22] G. Koutsoumbas, K. Ntrekis, E. Papantonopoulos, Gravitational Particle Production in Gravity Theories with Non-minimal Derivative Couplings. *JCAP* **08**, 027 (2013)
- [23] C. Germani, A. Kehagias, New Model of Inflation with Non-minimal Derivative Coupling of Standard Model Higgs Boson to Gravity. *Phys. Rev. Lett.* **105**, 011302 (2010)
- [24] C. Germani, Y. Watanabe, UV-protected (Natural) Inflation: Primordial Fluctuations and non-Gaussian Features. *JCAP* **1107**, 031 (2011). [Addendum: *JCAP*1107,A01(2011)]
- [25] L. Lombriser, A. Taylor, Breaking a Dark Degeneracy with Gravitational Waves. *JCAP* **1603**(03), 031 (2016)
- [26] L. Lombriser, N.A. Lima, Challenges to Self-Acceleration in Modified Gravity from Gravitational Waves and Large-Scale Structure. *Phys. Lett. B* **765**, 382 (2017)

- [27] D. Bettoni, J.M. Ezquiaga, K. Hinterbichler, M. Zumalacárregui, Speed of Gravitational Waves and the Fate of Scalar-Tensor Gravity. *Phys. Rev. D* **95**(8), 084029 (2017)
- [28] T. Baker, E. Bellini, P. G. Ferreira, M. Lagos, J. Noller and I. Sawicki, “Strong constraints on cosmological gravity from GW170817 and GRB 170817A,” *Phys. Rev. Lett.* **119**, no. 25, 251301 (2017) [arXiv:1710.06394 [astro-ph.CO]].
- [29] P. Creminelli and F. Vernizzi, “Dark Energy after GW170817 and GRB170817A,” *Phys. Rev. Lett.* **119**, no. 25, 251302 (2017) [arXiv:1710.05877 [astro-ph.CO]].
- [30] J. Sakstein and B. Jain, “Implications of the Neutron Star Merger GW170817 for Cosmological Scalar-Tensor Theories,” *Phys. Rev. Lett.* **119**, no. 25, 251303 (2017) [arXiv:1710.05893 [astro-ph.CO]].
- [31] J. M. Ezquiaga and M. Zumalacárregui, “Dark Energy After GW170817: Dead Ends and the Road Ahead,” *Phys. Rev. Lett.* **119**, no. 25, 251304 (2017) [arXiv:1710.05901 [astro-ph.CO]].
- [32] B. P. Abbott *et al.* [LIGO Scientific, Virgo, Fermi-GBM and INTEGRAL], “Gravitational Waves and Gamma-rays from a Binary Neutron Star Merger: GW170817 and GRB 170817A,” *Astrophys. J. Lett.* **848**, no.2, L13 (2017) [arXiv:1710.05834 [astro-ph.HE]].
- [33] C. Deffayet, S. Deser and G. Esposito-Farese, “Generalized Galileons: All scalar models whose curved background extensions maintain second-order field equations and stress-tensors,” *Phys. Rev. D* **80**, 064015 (2009) [arXiv:0906.1967 [gr-qc]].
- [34] Y. Gong, E. Papantonopoulos and Z. Yi, “Constraints on scalar-tensor theory of gravity by the recent observational results on gravitational waves,” *Eur. Phys. J. C* **78**, no. 9, 738 (2018) [arXiv:1711.04102 [gr-qc]].
- [35] S. Chakraborty, S. SenGupta, Solar system constraints on alternative gravity theories. *Phys. Rev. D* **89**(2), 026003 (2014)
- [36] N. Cruz, M. Olivares and J. R. Villanueva, “The Geodesic structure of the Schwarzschild anti-de Sitter black hole,” *Class. Quant. Grav.* **22** (2005), 1167-1190 [arXiv:gr-qc/0408016 [gr-qc]].
- [37] M. Vasudevan and K. A. Stevens, “Integrability of particle motion and scalar field propagation in Kerr-(Anti) de Sitter black hole spacetimes in all dimensions,” *Phys. Rev. D* **72** (2005) 124008 [gr-qc/0507096].
- [38] E. Hackmann and C. Lammerzahl, “Geodesic equation in Schwarzschild- (anti-) de Sitter space-times: Analytical solutions and applications,” *Phys. Rev. D* **78** (2008) 024035 [arXiv:1505.07973 [gr-qc]].
- [39] E. Hackmann and C. Lammerzahl, “Complete Analytical Solution of the Geodesic Equation in Schwarzschild-(Anti-) de Sitter Spacetimes,” *Phys. Rev. Lett.* **100** (2008) 171101 [arXiv:1505.07955 [gr-qc]].
- [40] M. Olivares, J. Saavedra, J. R. Villanueva and C. Leiva, “Motion of charged particles on the Reissner-Nordström (Anti-)de Sitter black holes,” *Mod. Phys. Lett. A* **26** (2011) 2923 [arXiv:1101.0748 [gr-qc]].
- [41] N. Cruz, M. Olivares, J. Saavedra and J. R. Villanueva, “Null geodesics in the Reissner-Nordstrom Anti-de Sitter black holes,” arXiv:1111.0924 [gr-qc].
- [42] A. Larranaga, “Geodesic Structure of the Noncommutative Schwarzschild Anti-de Sitter Black Hole I: Timelike Geodesics,” *Rom. J. Phys.* **58** (2013) 50 [arXiv:1110.0778 [gr-qc]].
- [43] J. R. Villanueva, J. Saavedra, M. Olivares and N. Cruz, “Photons motion in charged Anti-de Sitter black holes,” *Astrophys. Space Sci.* **344** (2013) 437.
- [44] P. A. Gonzalez, E. Papantonopoulos, J. Saavedra and Y. Vasquez, ‘Four-Dimensional Asymptotically AdS Black Holes with Scalar Hair,’ *JHEP* **1312** (2013) 021 [arXiv:1309.2161 [gr-qc]].
- [45] P. A. Gonzalez, M. Olivares and Y. Vasquez, “Motion of particles on a Four-Dimensional Asymptotically AdS Black Hole with Scalar Hair,” *Eur. Phys. J. C* **75**, no. 10, 464 (2015) [arXiv:1507.03610 [gr-qc]].
- [46] S. Bhattacharya, S. Chakraborty, Constraining some Horndeski gravity theories. *Phys. Rev. D* **95**(4), 044037 (2017)
- [47] P. A. González, M. Olivares, E. Papantonopoulos and Y. Vásquez, “Constraints on scalar-tensor theory of gravity by solar system tests,” *Eur. Phys. J. C* **80** (2020) no.10, 981 [arXiv:2002.03394 [gr-qc]].
- [48] A. I. Vainshtein, “To the problem of nonvanishing gravitation mass,” *Phys. Lett.* **B39**, 393-394 (1972).
- [49] E. Babichev and C. Deffayet, “An introduction to the Vainshtein mechanism,” arXiv:1304.7240 [gr-qc].
- [50] K. Koyama, G. Niz, G. Tasinato, "Analytic solutions in non-linear massive gravity". *Phys. Rev. Lett.* **107**, 131101 (2011) [arXiv:1103.4708 [hep-th]]; K. Koyama, G. Niz, G. Tasinato, "Strong interactions and exact solutions in non-linear massive gravity", *Phys. Rev. D* **84**, 064033 (2011) [arXiv:1104.2143 [hep-th]]; K. Koyama, G. Niz and G. Tasinato, “Effective theory for the Vainshtein mechanism from the Horndeski action,” *Phys. Rev. D* **88**, 021502 (2013) [arXiv:1305.0279 [hep-th]].
- [51] R. Kimura, T. Kobayashi and K. Yamamoto, “Vainshtein screening in a cosmological background in the most general second-order scalar-tensor theory,” *Phys. Rev. D* **85**, 024023 (2012) [arXiv:1111.6749 [astro-ph.CO]].
- [52] A. De Felice, R. Kase, S. Tsujikawa, Vainshtein mechanism in second-order scalar-tensor theories. *Phys. Rev. D* **85**, 044059 (2012).
- [53] R. Kase and S. Tsujikawa, “Screening the fifth force in the Horndeski’s most general scalar-tensor theories,” *JCAP* **1308**, 054 (2013) [arXiv:1306.6401 [gr-qc]].
- [54] R. S. Kuniyal, R. Uniyal, H. Nandan and K. D. Purohit, “Null Geodesics in a Magnetically Charged Stringy Black Hole Spacetime,” *Gen. Rel. Grav.* **48**, no.4, 46 (2016) [arXiv:1509.05131 [gr-qc]].
- [55] S. Soroushfar, R. Saffari and E. Sahami, “Geodesic equations in the static and rotating dilaton black holes: Analytical solutions and applications,” *Phys. Rev. D* **94**, no.2, 024010 (2016) [arXiv:1601.03143 [gr-qc]].
- [56] D. Garfinkle, G. T. Horowitz and A. Strominger, “Charged black holes in string theory,” *Phys. Rev. D* **43**, 3140 (1991) [erratum: *Phys. Rev. D* **45**, 3888 (1992)]
- [57] D. Amaro and A. Macías, “Geodesic structure of the Euler-Heisenberg static black hole,” *Phys. Rev. D* **102**, no.10, 104054 (2020)
- [58] D. Chen and C. Gao, “Angular momentum and chaos bound of charged particles around Einstein–Euler–Heisenberg AdS black holes,” *New J. Phys.* **24**, no.12, 123014 (2022) [arXiv:2205.08337 [hep-th]].
- [59] V. Cardoso, A. S. Miranda, E. Berti, H. Witek and V. T. Zanchin, “Geodesic stability, Lyapunov exponents and quasinormal modes,” *Phys. Rev. D* **79** (2009) no.6,

- 064016 [arXiv:0812.1806 [hep-th]].
- [60] R. C. Myers and M. J. Perry, “Black Holes in Higher Dimensional Space-Times,” *Annals Phys.* **172**, 304 (1986)
- [61] F. Pretorius and D. Khurana, “Black hole mergers and unstable circular orbits,” *Class. Quant. Grav.* **24**, S83-S108 (2007) [arXiv:gr-qc/0702084 [gr-qc]].
- [62] U. Sperhake, V. Cardoso, F. Pretorius, E. Berti and J. A. Gonzalez, “The High-energy collision of two black holes,” *Phys. Rev. Lett.* **101**, 161101 (2008) [arXiv:0806.1738 [gr-qc]].
- [63] M. Shibata, H. Okawa and T. Yamamoto, “High-velocity collision of two black holes,” *Phys. Rev. D* **78**, 101501 (2008) [arXiv:0810.4735 [gr-qc]].
- [64] E. Babichev, C. Charmousis and A. Lehébel, “Asymptotically flat black holes in Horndeski theory and beyond,” *JCAP* **04** (2017), 027 [arXiv:1702.01938 [gr-qc]].
- [65] S. Chandrasekhar, “The mathematical theory of black holes”, Oxford University Press, 2002.
- [66] J. R. Villanueva, F. Tapia, M. Molina and M. Olivares, “Null paths on a toroidal topological black hole in conformal Weyl gravity,” *Eur. Phys. J. C* **78** (2018) no.10, 853 [arXiv:1808.04298 [gr-qc]].
- [67] Wald R.M.: General relativity. The University Chicago Press, Chicago (1984).
- [68] P. A. González, M. Olivares, Y. Vásquez and J. R. Villanueva, “Null geodesics in five-dimensional Reissner-Nordström anti-de Sitter black hole,” *Eur. Phys. J. C* **81** (2021) no.3, 236 [arXiv:2010.01442 [gr-qc]].
- [69] N. Straumann, “General relativity and relativistic astrophysics”, Springer, Berlin, 1984.
- [70] V. Kagramanova, J. Kunz and C. Lammerzahl, “Solar system effects in Schwarzschild-de Sitter spacetime,” *Phys. Lett. B* **634**, 465 (2006) [gr-qc/0602002].
- [71] S. S. Shapiro, J. L. Davis, D. E. Lebach and J. S. Gregory, “Measurement of the Solar Gravitational Deflection of Radio Waves using Geodetic Very-Long-Baseline Interferometry Data, 1979-1999,” *Phys. Rev. Lett.* **92**, 121101 (2004).
- [72] R. F. C. Vessot *et al.*, “Test of Relativistic Gravitation with a Space-Borne Hydrogen Maser,” *Phys. Rev. Lett.* **45**, 2081 (1980).
- [73] P. Pradhan, “Stability analysis and quasinormal modes of Reissner–Nordström space-time via Lyapunov exponent,” *Pramana* **87** (2016) no.1, 5 [arXiv:1205.5656 [gr-qc]].
- [74] P. P. Pradhan, “Lyapunov Exponent and Charged Myers Perry Spacetimes,” *Eur. Phys. J. C* **73** (2013) no.6, 2477 [arXiv:1302.2536 [gr-qc]].
- [75] J. Maldacena, S. H. Shenker and D. Stanford, “A bound on chaos,” *JHEP* **08** (2016), 106 [arXiv:1503.01409 [hep-th]].
- [76] S. H. Shenker and D. Stanford, “Black holes and the butterfly effect,” *JHEP* **03** (2014), 067 [arXiv:1306.0622 [hep-th]].
- [77] S. H. Shenker and D. Stanford, “Multiple Shocks,” *JHEP* **12** (2014), 046 [arXiv:1312.3296 [hep-th]].
- [78] J. M. Maldacena, “The Large N limit of superconformal field theories and supergravity,” *Adv. Theor. Math. Phys.* **2** (1998), 231-252 [arXiv:hep-th/9711200 [hep-th]].